Bipolar Photothermoelectric Effect Across Energy Filters in Single Nanowires

Steven Limpert[1,2*], Adam Burke[1], I-Ju Chen[1], Nicklas Anttu[1], Sebastian Lehmann[1], Sofia Fahlvik[1], Stephen Bremner[2], Gavin Conibeer[2], Claes Thelander[1], Mats-Erik Pistol[1] and Heiner Linke[1*]

[1]NanoLund and Solid State Physics, Lund University, Box 118, 22100 Lund, Sweden

[2]School of Photovoltaic and Renewable Energy Engineering, University of New South Wales, 2052 Sydney, Australia

[*]email: steven.limpert@ftf.lth.se, heiner.linke@ftf.lth.se

Supporting Information

Photothermoelectric Effects

Two different types of PTE effect results are commonly reported, which vary in physical mechanism, but which are not differentiated in nomenclature. To clarify the area in which we report results, we will discuss these two types briefly here, calling them the lattice-gradient PTE effect and the carrier-gradient PTE effect, respectively.

In the lattice gradient PTE effect, the carriers within a certain volume of the lattice have the same temperature as that volume of the lattice.[1] In this case, the thermal gradient which drives the PTE effect is a lattice temperature gradient. This lattice temperature gradient is produced by the non-uniform absorption of light because photogenerated carriers dissipate their excess kinetic energy to the lattice by phonon emission, heating the lattice more in volumes of stronger absorption. The lattice gradient PTE effect is similar to conventional thermoelectrics as carrier and lattice temperature are identical. Similar to traditional thermoelectrics, the temperature gradient that can be sustained is limited by phonon heat flow through the lattice.[2]

In the carrier-gradient PTE effect, the photogenerated carriers within a certain volume of the lattice have a different temperature than that volume of the lattice. In this case, the thermal gradient that drives the PTE effect is a carrier temperature gradient that exists between the hot photogenerated carriers present in regions of absorption and the lattice-temperature carriers present in regions of no absorption. Photogenerated carriers are out of thermal equilibrium with the lattice for picoseconds after generation,[3] can remain hot for longer when their dissipation of excess kinetic energy is inhibited,[4–6] and can dominate photoresponse.[7,8] Using the carrier gradient PTE effect, larger temperature gradients can be sustained between the photogenerated carriers and the lattice, and between the photogenerated carriers and the lattice-temperature carriers in non-absorbing volumes. This is because in such systems, the lattice may remain at a more or less uniform temperature, eliminating thermal equilibration by photon heat flow.

In this work, we report results of the carrier-gradient type.

Carrier Energy Filtering and the Seebeck Coefficient

Carrier-energy filtering provides a means to control the Seebeck coefficient of the system because the Seebeck coefficient is a description of the entropy per unit charge carried by a current. As an electron's entropy is given by the difference of its energy and its quasi-Fermi level divided by its temperature, $(E - E_{Fn})/T$, the Seebeck coefficient of an ensemble of electrons can be modified by varying the energy spectrum of electrons which contribute to thermoelectric transport. Since the Seebeck coefficient is proportional to the average kinetic energy of carriers transmitted by an energy filter,[9] by employing an energy filter which only allows electrons with energies much greater than the electron quasi-Fermi level to contribute to transport, the Seebeck coefficient can be increased.

Nanowire characterization

We present information in support of our assertion that the InAs/InP double heterostructure nanowires utilized in the experiments presented in the main text exhibited atomically precise interfaces, low defect densities and were of wurtzite crystal phase.

Eleven nanowires from the same growth batch as used for the experiment were characterized by transmission electron microscopy (TEM), high-resolution transmission electron microscopy (HRTEM), and scanning TEM – high angle annular dark field microscopy (STEM-HAADF). InAs/InP interface abruptness, crystal quality, crystal structure and layer thickness distributions were determined. The average, maximum and minimum layer thicknesses (as labeled in Figure S1) are presented in Table S1. Data on the layer thickness of the InAs layer to the right of the InP single barrier is not included as this segment length depended randomly on where the wires broke off from the substrate. HRTEM analysis showed that the InAs/InP interfaces were atomically sharp (Figs. S2a-c). Additionally, the crystal quality was found to be high - only a few stacking faults being detectable (Fig. S2d) - and the crystal structure of the InAs and InP was found to be wurtzite (Fig. S2e).

	Average Length (nm)	Maximum Length (nm)	Minimum Length (nm)
InP Single Barrier	41	60	26
InAs Segment 1	266	320	194
InP Double Barrier	4	8	2
InAs Quantum Dot	17	19	16
InAs Segment 2	356	437	293

Table S1 | Geometrical analysis of TEM micrographs of 11 nanowires.

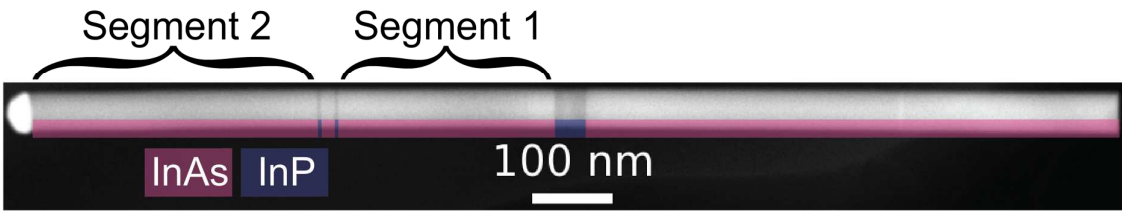

Figure S1 | STEM-HAADF micrograph of an InAs/InP heterostructure nanowire with segment labels.

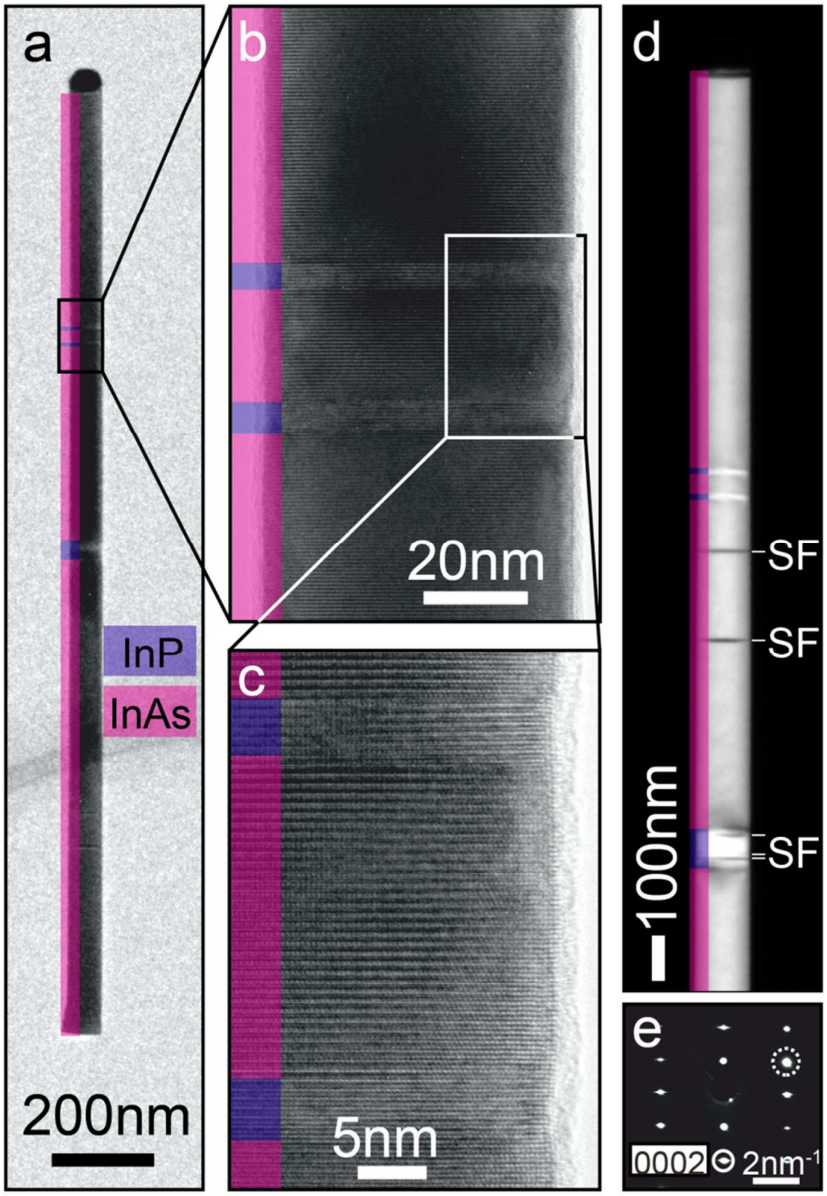

Figure S2 | TEM and HRTEM characterization of nanowires. a, Transmission electron microscopic bright field overview image of an InAs/InP axial heterostructure nanowire including a single and double InP barrier structure embedded in InAs segments. **b and c,** Higher magnification inset of the InP axial double segment/barrier and high resolution (HR)TEM image of the same section of the nanowire, respectively. **d,** Conventional TEM dark field image using the wurtzite crystal structure selective diffraction spot for imaging (highlighted by the dotted ring in (**e**) resulting in high contrast for wurtzite area and low contrast for stacking faults (SF). **e,** Selected area diffraction pattern (SADP) taken along a ⟨110⟩-type direction of the nanowire shown in (**a**) highlighting the wurtzite crystal structure characteristic diffraction pattern. InP and InAs axial segments are false colored in (**a**) to (**d**) (InAs – pink, InP – violet) as a guide to the eye.

Wave Optics Model

We present information regarding the COMSOL wave optics simulations performed to support our argument that the wavelength dependence of the location and intensity of absorption hot spots is the cause of the photoresponse reversals exhibited by the devices presented in the main text.

First, we present calculations of the normalized absorption rate density, *G*, within a uniform InAs, 1.5 μm long, 60 nm diameter, single nanowire placed on a SiO_2 substrate (Fig. S3a) under global illumination for wavelengths from 0.5 μm to 1.0 μm (Fig. S3b). These results show that the electric field magnitude, and correspondingly, the absorption, is non-uniform within the wire and that the maxima of the optical modes within the nanowire into which the light couples spatially shift as the wavelength of light changes. The explanation for this result is that the solution to the wave equation depends upon the wavenumber, k, and the complex permittivity of the material, which are wavelength-dependent parameters.

Next, we present calculations in which we insert the heterostructures into the model (Fig. S2c) and calculate the normalized absorption rate density, *G*, within a heterostructure InAs/InP nanowire (Fig. S2d). These results show that the presence of the heterostructures does not significantly change the electric field magnitude, and correspondingly, the absorption, from the uniform InAs nanowire case. The explanation for this result is that the volumes of InP are small and the difference between the permittivities of InAs and InP are also small. Because the electric field magnitude does not depend strongly upon the heterostructure position, it is possible to realize 1) a scenario in which absorption is asymmetric about a heterostructure (in which case, a PTE effect is expected) or 2) a scenario in which absorption is symmetric about a heterostructure (in which case, a PTE effect is not expected) by placing the heterostructure at a selected location. In the presented case (Fig. S2d), the double-barrier is located such that absorption on either side of it is asymmetric, and the single-barrier is located such that absorption on either side of it is symmetric. In the symmetric absorption case, no PTE effect would be expected – only a photoconductive effect.

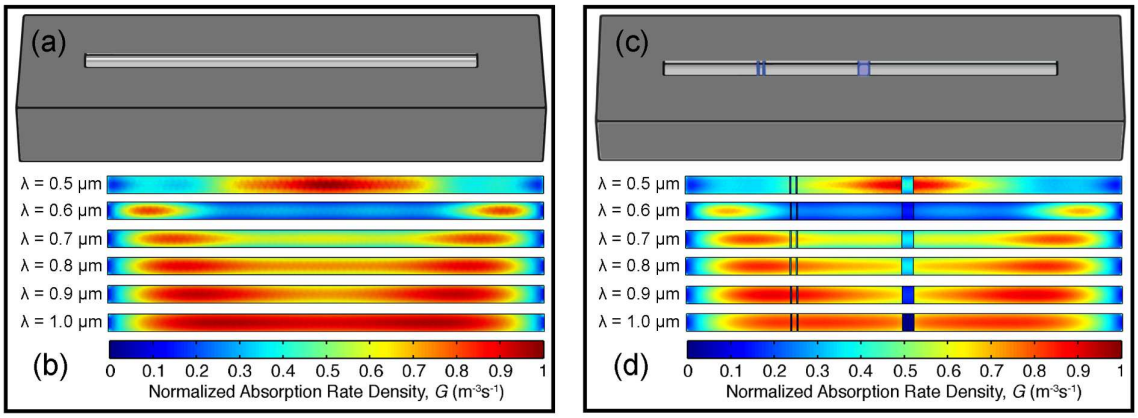

Figure S3 | Electromagnetic wave modelling. (a) 3D model geometry of 1.5 μm long, 60 nm diameter, InAs nanowire on SiO_2 substrate. (b) Cross-sections of the normalized absorption rate density, *G*, along the widest point of the InAs nanowire in (a) for randomly polarized light of wavelengths as indicated. (c) 3D model geometry of 1.5 μm long, 60 nm diameter, InAs/InP heterostructure nanowire on SiO_2 substrate. A 40 nm single InP segment is present at one-half of the nanowire's length and a InP-InAs-InP double-barrier heterostructure of 4.5 nm, 17nm and 4.5 nm segment lengths is present at one-quarter of the nanowire's length. (d) Cross-sections of the normalized absorption rate density, *G*, along the widest point of the InAs/InP heterostructure

nanowire in (c) for randomly polarized light of wavelengths as indicated. Absorption is symmetric about the single barrier and asymmetric about the double-barrier.

The refractive index of the SiO_2 substrate was taken to be wavelength independent and equal to 1.5 and at the rear of the substrate, a perfectly matched layer was present. Bulk zinc blende refractive index data was used for the InAs and InP segments (Figure S4). Importantly, variations between the complex refractive indices of zinc blende and wurtzite InAs are not expected to be substantial at wavelengths greater than 500 nm[10] and the volume of InP is small. Therefore, no issues are anticipated with the use of the bulk zinc blende refractive index data.

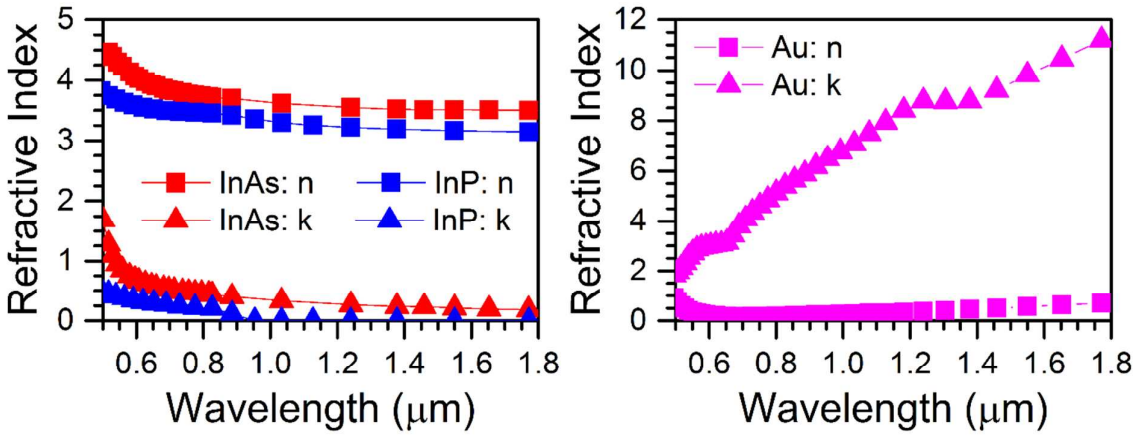

Figure S4 | Complex refractive index data. a, InAs and InP. **b,** Au.

Ohmic Contact to InAs

We present information in support of our argument that photocurrent collection in our devices is not due to the presence of unintentional Schottky contacts.

Identical contacts to those used in the devices presented in the main work were fabricated on pure InAs nanowire segments and dark IV curves were measured. The linearity of the dark IV curves (Figure S5) indicates that Ohmic contact was made to the InAs nanowire and that Schottky contacts are not present.

Due to the low resistivity of the pure InAs wires, it was not feasible with the low-current measurement setup used for our experiments to measure the large current that would have been present at larger source-drain voltages. However, in previous and subsequent experiments using pure InAs wires contacted by the same method, we have measured the current-voltage curves out to such large source-drain voltages on a different measurement setup and the curves remain linear. We are highly confident in the Ohmic contact due to these results and due to the fact that making Ohmic contact to InAs is a well-established process in the lab in which the devices were fabricated.[11]

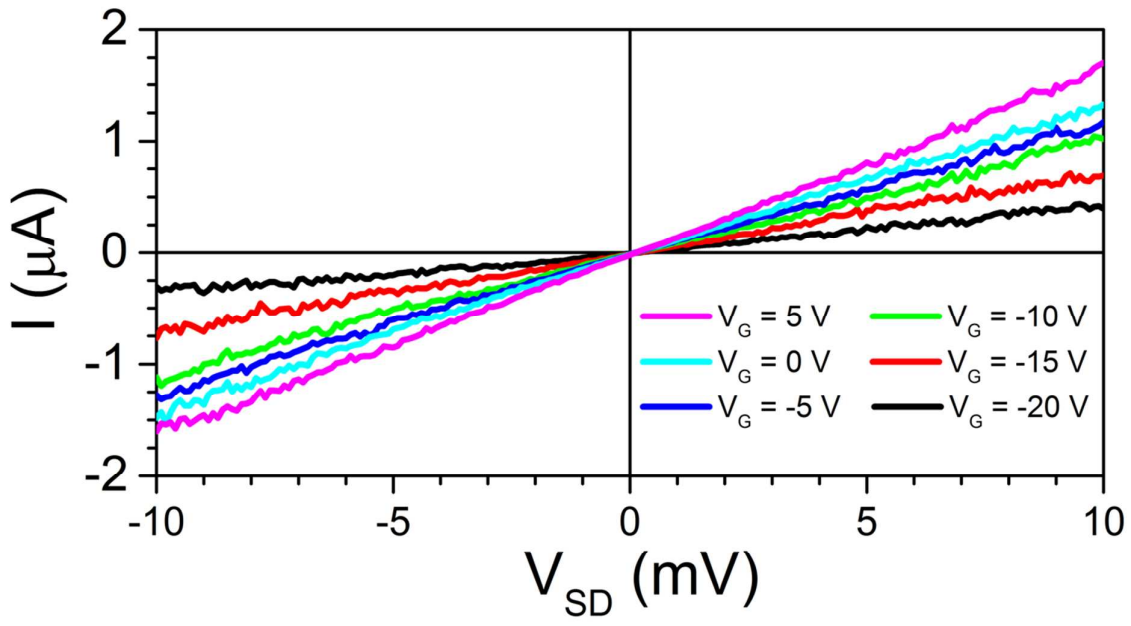

Figure S5 | Dark source-drain IV curves of a plain InAs nanowire as a function gate voltage, V_G.

Power of Narrowband Light as a Function of Center Wavelength

The power of the narrowband light was measured using a Thorlabs power meter and silicon and germanium photodiodes (Thorlabs item numbers PM100D, S120C and S122C). Variation of power with center wavelength is because (i) the supercontinuum source did not emit exactly the same amount of power at each wavelength and (ii) the monochromator gratings (800 nm blaze, 150 g/mm) had efficiencies which varied with wavelength.

While variation in power results in variation in photocurrent magnitude in cases of asymmetric absorption (or variation in photoconductivity magnitude in the case of symmetric absorption), it does not affect the shape of the absorption distribution itself or result in variation in the PTE sign. Therefore, we do not attribute our observation of reversals in PTE sign with wavelength to variation in power with wavelength.

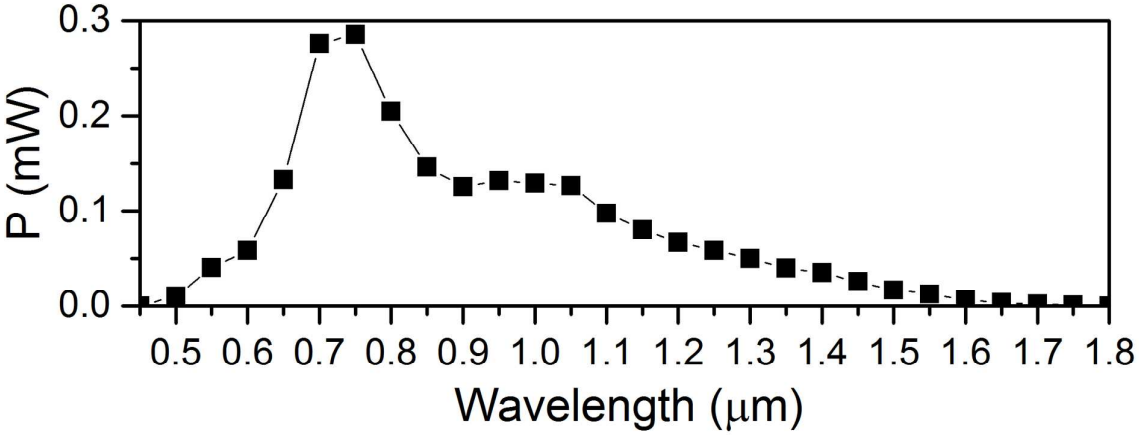

Figure S6 | Power of narrowband light as a function of center wavelength.

Conductance Curve of Double Barrier Device

Figure S7 presents the dark, low temperature conductance curve of a double-barrier, single-nanowire device at a source-drain voltage of 1 mV. The conductance data exhibits oscillations indicative of resonances related to the quantum nature of the double-barrier transmission spectrum and shows that a positive gate voltage is necessary to turn on the n-type conductivity of the device at low temperature.

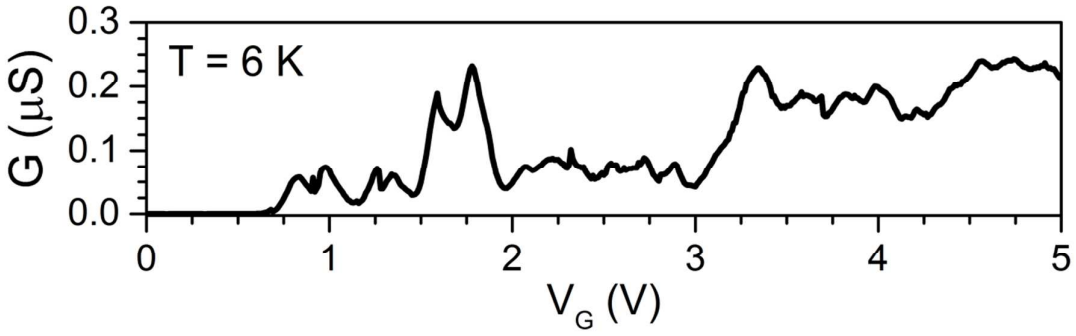

Figure S7 | Double barrier device conductance curve at V_{SD} = 1 mV.

Bibliography

(1) Léonard, F.; Song, E.; Li, Q.; Swartzentruber, B.; Martinez, J. A.; Wang, G. T. *Nano Lett.* **2015**, *15* (12), 8129–8135.
(2) Hamid Elsheikh, M.; Shnawah, D. A.; Sabri, M. F. M.; Said, S. B. M.; Haji Hassan, M.; Ali Bashir, M. B.; Mohamad, M. *Renew. Sustain. Energy Rev.* **2014**, *30*, 337–355.
(3) Shah, J. *Ultrafast Spectroscopy in Seminconductors and Semiconductor Nanostructures*, 2nd ed.; Springer Series in Solid-State Sciences; Springer: Berlin, Heidelberg, 1999; Vol. 115.
(4) Bistritzer, R.; MacDonald, A. H. *Phys. Rev. Lett.* **2009**, *102* (20).
(5) Wang, Y.; Jackson, H. E.; Smith, L. M.; Burgess, T.; Paiman, S.; Gao, Q.; Tan, H. H.; Jagadish, C. *Nano Lett.* **2014**, *14* (12), 7153–7160.
(6) Tedeschi, D.; De Luca, M.; Fonseka, H. A.; Gao, Q.; Mura, F.; Tan, H. H.; Rubini, S.; Martelli, F.; Jagadish, C.; Capizzi, M.; Polimeni, A. *Nano Lett.* **2016**, *16* (5), 3085–3093.
(7) Gabor, N. M.; Song, J. C. W.; Ma, Q.; Nair, N. L.; Taychatanapat, T.; Watanabe, K.; Taniguchi, T.; Levitov, L. S.; Jarillo-Herrero, P. *Science* **2011**, *334* (6056), 648.
(8) Sun, D.; Aivazian, G.; Jones, A. M.; Ross, J. S.; Yao, W.; Cobden, D.; Xu, X. *Nat. Nanotechnol.* **2012**, *7* (2), 114–118.
(9) Ali Shakouri Edwin Y. Lee D. L. Smi. *Microscale Thermophys. Eng.* **1998**, *2* (1), 37–47.
(10) Anttu, N.; Lehmann, S.; Storm, K.; Dick, K. A.; Samuelson, L.; Wu, P. M.; Pistol, M.-E. *Nano Lett.* **2014**, *14* (10), 5650–5655.
(11) Suyatin, D. B.; Thelander, C.; Björk, M. T.; Maximov, I.; Samuelson, L. *Nanotechnology* **2007**, *18* (10), 105307.